JACS
JOURNAL OF THE AMERICAN CHEMICAL SOCIETY
Article
Cite This: J. Am. Chem. Soc. 2019, 141, 3288−3297
pubs.acs.org/JACS

Catalytic Enantioselective Hetero-[6+4] and -[6+2] Cycloadditions for the Construction of Condensed Polycyclic Pyrroles, Imidazoles, and Pyrazoles

Giulio Bertuzzi,[†] Mathias Kirk Thøgersen,[†] Maxime Giardinetti,[†] Andreu Vidal-Albalat,[†] Adam Simon,[‡,§] K. N. Houk,*[,‡,§] and Karl Anker Jørgensen*[,†]

[†]Department of Chemistry, Aarhus University, DK-8000 Aarhus C, Denmark

[‡]Department of Chemistry and Biochemistry and [§]Department of Chemical and Biomolecular Engineering, University of California, Los Angeles, California 90095, United States

Supporting Information

ABSTRACT: The development of the first chemo-, regio-, and stereoselective hetero-[6+4] and -[6+2] cycloadditions of heteroaromatic compounds via amino aza- and diazafulvenes is presented. Pyrroles, imidazoles, and pyrazoles substituted with a formyl group react with an aminocatalyst to generate an electron-rich hetero-6π-component that reacts in a chemo-, regio-, and stereoselective manner with electron-deficient dienes and olefins. For the hetero-[6+4] cycloaddition of the pyrrole system with dienes, a wide variation of both reaction partners is possible, providing attractive pyrrolo-azepine products in high yields and excellent enantioselectivities (99% ee). The hetero-[6+4] cycloaddition reaction concept is extended to include imidazoles and pyrazoles, giving imidazolo- and pyrazolo-azepines. The same activation concept is successfully employed to include hetero-[6+2] cycloadditions of the pyrrole system with nitroolefins, giving important pyrrolizidine-alkaloid scaffolds. Experimental NMR and mechanistic studies allowed for the identification of two different types of intermediates in the reaction. The first intermediate is the result of a rapid formation of an iminium ion, which generates a hetero-6π aminofulvene intermediate as a mixture of two isomers. Density functional theory calculations were used to determine the mechanism and sources of asymmetric induction in the hetero-[6+4] and -[6+2] cycloadditions. After formation of the reactive hetero-6π-components, a stepwise addition occurs with the diene or olefin, leading to a zwitterionic intermediate that undergoes cyclization to afford the cycloadduct, followed by eliminative catalyst release. The stereoselectivity is controlled by the second step, and computations elaborate on the various substrate and catalyst effects that alter the experimentally observed enantioselectivities. The computational studies provided a basis for improving the enantioselectivity of the hetero-[6+2] cycloaddition.

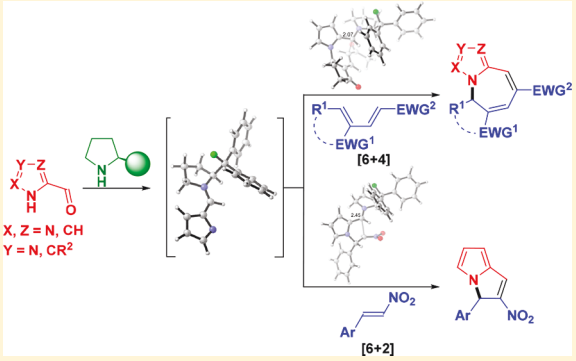

INTRODUCTION

Expanding the borders of reactivity can pave avenues for novel methodologies in organic synthesis. An important challenge for such new developments is to provide methodologies where basic organic molecules are employed in combination with diverse reaction partners. Furthermore, combining experimental and computational investigations might provide deeper mechanistic understandings for expanding reactivity into new chemical spaces. In the following, we present the unprecedented catalytic chemo-, regio-, and enantioselective hetero-[6+4] and -[6+2] cycloaddition reactions of heteroaromatic compounds. Mechanistic studies allow for identification of reactive intermediates in the catalytic cycle. Computational studies afford important insights into the mechanism and stereoselectivity of these cycloaddition reactions and allow for improvement of enantioselectivity.

Heterocyclic compounds, such as pyrroles, imidazoles, and pyrazoles, are fundamental scaffolds in chemistry. Their functionalization has been the center of numerous synthetic efforts, due to their presence in, e.g., biologically relevant compounds[1−5] and materials.[6−9] Functionalization of these heterocyclic compounds is usually carried out through electrophilic *C*-functionalizations, for which a large number of well-established methodologies exist.[10] Besides classical electrophilic aromatic substitution reactions, such as halogenation, nitration, sulfonation, acylation, and Vilsmeier−Haack formylation, enantioselective functionalization of pyrrole derivatives has mainly been carried out under Friedel−Crafts conditions[11,12] or following C−H functionalization methodologies (Scheme 1, top).[13] Only one example of an aldehyde

Received: December 21, 2018
Published: February 12, 2019

DOI: 10.1021/jacs.8b13659
J. Am. Chem. Soc. 2019, 141, 3288−3297

Scheme 1. *N*- versus *C*-Asymmetric Functionalization of Pyrrole Derivatives

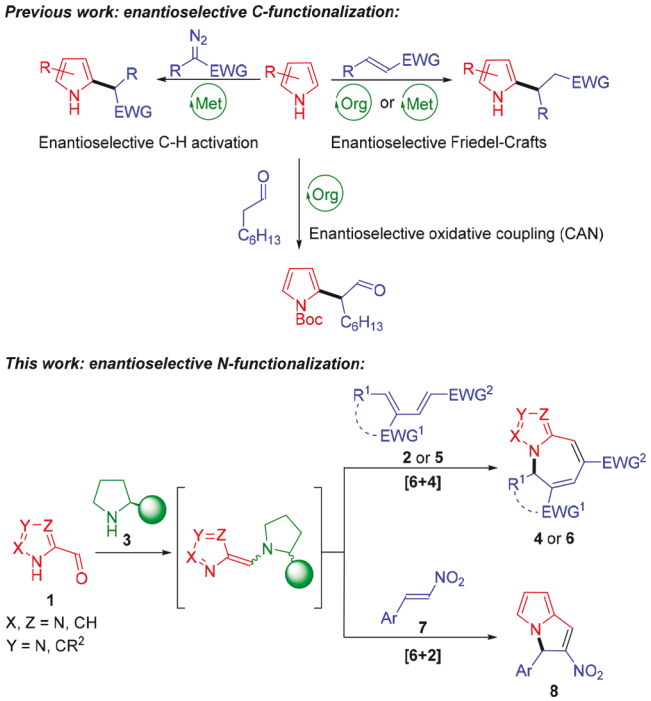

(octanal) reacting with *N*-Boc pyrrole under organocatalytic oxidative conditions has been reported[14] (Scheme 1, top). On the other hand, the employment of pyrroles and related heteroaromatic compounds as *N*-centered nucleophiles is much less explored, although *N*-fused bicycles are key backbones of many important products.[15−20]

In the present work, we disclose novel direct strategies for enantioselective functionalization of pyrroles, imidazoles, and pyrazoles based on unprecedented catalytic enantioselective hetero-[6+4] and -[6+2] cycloaddition reactions (Scheme 1, bottom). Mechanistic studies based on NMR and computational investigations provide valuable information about catalytic intermediates, reaction courses, and how to improve the stereoselective performance of the catalyst.

Recently, the first intermolecular organocatalytic enantioselective [6+4],[21] [8+2],[22,23] and [10+4] cycloadditions[24] were disclosed. In addition, Hayashi reported an intramolecular [6+2] cycloaddition of a fulvene moiety with a catalytically generated enamine.[25] Hong explored the use of 6-aminofulvenes in stoichiometric amounts for intermolecular [6+2],[26] [6+3],[27] and [6+4] cycloadditions.[28] Furthermore, Chen developed an organocatalyzed enantioselective [6+2] cycloaddition where a 4-aminofulvene intermediate is produced *in situ* in catalytic quantities.[29]

Pyrroles, imidazoles, and pyrazoles, substituted with a formyl group, are stable aromatic species that, upon condensation with an aminocatalyst, give aminoazafulvenes.[30,31] These 6π-components are expected to be prone to participate in cycloadditions. Stable 6-aminoazafulvenes were first reported in 1975 by Kanemasa,[32] and later 6-amino-1,4-diazafulvene was shown to react as a 6π-component in thermal[33] and metal-promoted[34] cycloadditions.

To the best of our knowledge, pyrrole, imidazole, and pyrazole derivatives have never been demonstrated to participate in enantioselective hetero-[6+4] cycloadditions, and only few examples of racemic hetero-[6+2] cycloadditions have been disclosed.[32−34] The nitrogen-containing bicyclic compounds obtained with the presented methodology (Scheme 1, bottom) include pyrrolo[1,2-*a*]azepines **4** or **6** and pyrrolizine derivatives **8**. The former is a part of the scaffold in the family of Stemona alkaloids, like Parvistemonine A **A**[35] and cephalotaxine alkaloids **B**.[36] Furthermore, Midazolam **C** and related imidazobenzodiazepine-based anti-anxiety drugs,[37] present a similar backbone built on a diazole moiety. Compounds **8** contain a skeleton shared between a family of recurring natural pyrrolizidine alkaloids **D** exhibiting cytotoxicity.[38] In addition, this motif is present in Ketorolac, a non-steroidal anti-inflammatory drug **E** (Figure 1).[39]

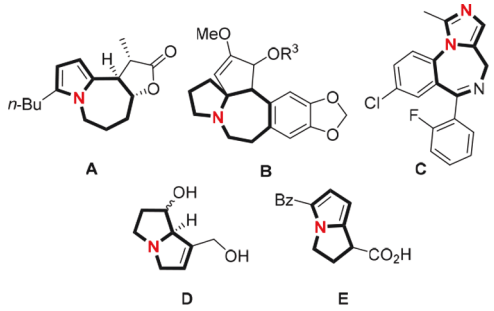

Figure 1. Biologically relevant scaffolds **A**−**E** based on products **4**, **6**, and **8** in Scheme 1.

RESULTS AND DISCUSSION

Screening of Reaction Conditions for Hetero-[6+4] Cycloadditions. We started our investigation by treating pyrrole-2-carbaldehyde **1a** with secondary aminocatalysts **3** to provide the desired transient electron-rich 6-aminoazafulvene which was captured by electron-deficient diene **2a** in a hetero-[6+4] cycloaddition, rendering the tricyclic compound **4aa** after catalyst release. The most commonly employed aminocatalyst **3a**[40,41] combined with benzoic acid (BzOH) and molecular sieves (MS) as additives in dry $CDCl_3$ at room temperature delivered **4aa** in trace amounts, but with an excellent degree of enantioselectivity (99% ee, Table 1, entry 1). Changing for a less bulky fluorine substituted catalyst **3b**[42,43] improved the yield to 40% maintaining the enantioselectivity (entry 2), while catalyst **3c** afforded **4aa** with improved yield but slightly diminished enantioselectivity (entry 3). The most stereoselective catalyst was selected and, in order to overcome the poor reactivity, other reaction parameters were evaluated. Notably, to achieve a decent degree of conversion, both BzOH and molecular sieves (MS) have to be applied as additives (entries 4 and 5). Performing the reaction at 40 °C resulted in diminished yield due to rapid decomposition of **2a** (entry 6). However, employing an excess of **2a** improved the yield slightly (entry 7). Finally, after additional screening (see Supporting Information), we found that *p*MeOBzOH, along with a more concentrated reaction medium and a reaction time of 2 days, afforded **4aa** in 73% yield and 99% ee (entry 8).

Scope of Hetero-[6+4] Cycloadditions for Pyrroles. First, variations of substituents in the 4-position of the pyrrole ring were explored. The introduction of heteroatoms such as bromine (**1b**), silicon (**1c**), and sulfur (**1d**) provided the products **4ba**−**da** in 68−90% yield and 99% ee (Table 2, entries 2−4). The absolute configuration of **4da** was assigned

DOI: 10.1021/jacs.8b13659
J. Am. Chem. Soc. 2019, 141, 3288−3297

Table 1. Optimization of the Hetero-[6+4] Cycloaddition[a]

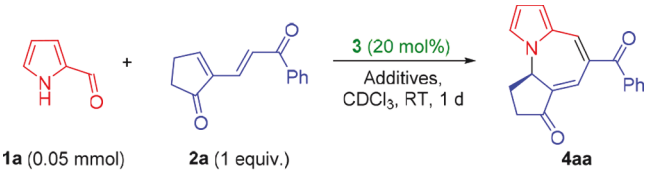

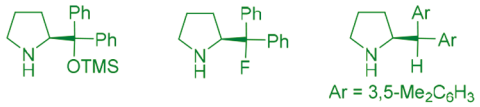

3a 3b 3c

entry	cat. 3	additive[b]	yield (%)[c]	ee (%)[d]
1	3a	BzOH, MS	5	99
2	3b	BzOH, MS	40	99
3	3c	BzOH, MS	65	95
4	3b	MS	12	n.d.
5	3b	BzOH	10	n.d.
6[e]	3b	BzOH, MS	20	96
7[f]	3b	BzOH, MS	46	99
8[f]	3b	*p*MeOBzOH, MS	75(73)[g]	99

[a]Reaction conditions: see Supporting Information. [b]20 mol% acid used. [c]Yield measured by NMR on the crude reaction mixture with Et_4Si as internal standard. [d]Determined by chiral stationary phase UPCC. [e]Reaction at 40 °C. [f]Reaction conditions: **1a** (0.1 mmol), **2a** (0.15 mmol), 2 d. [g]Isolated yield.

Table 2. Reaction Scope of the Hetero-[6+4] Cycloaddition: Variation of Aldehydes 1 and Electron-Poor Dienes 2[a]

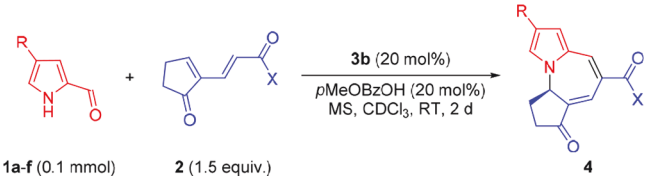

entry	1, R	2, X	4, yield (%)[b]	ee (%)[c]
1	**1a**, H	**2a**, Ph	**4aa**, 73	99
2	**1b**, Br	**2a**, Ph	**4ba**, 68	99
3	**1c**, $Si(iPr)_3$	**2a**, Ph	**4ca**, 90	99
4	**1d**, SPh	**2a**, Ph	**4da**, 70	99
5	**1e**, Ph	**2a**, Ph	**4ea**, 65	99
6	**1f**, *p*MeOC$_6$H$_4$	**2a**, Ph	**4fa**, 52	99
7	**1a**, H	**2b**, *p*BrC$_6$H$_4$	**4ab**, 87	99
8	**1a**, H	**2c**, *p*MeOC$_6$H$_4$	**4ac**, 54	99
9	**1a**, H	**2d**, *p*NO$_2$C$_6$H$_4$	**4ad**, 67	99
10	**1a**, H	**2e**, OEt	**4ae**, 60	99
11	**1a**, H	**2f**, OPh	**4af**, 88	99

[a]Reaction conditions: Supporting Information. [b]Isolated yield. [c]Determined by chiral stationary phase UPCC.

by single-crystal X-ray analysis (see Supporting Information) and extended by analogy to products **4** and **6** (*vide infra*). An aromatic substituent (aldehydes **1e** and **1f**) gave **4ea** and **4fa** with similarly high yields and excellent stereoselectivities (entries 5 and 6). Modifications on the electron-withdrawing group of **2** were then explored, finding that different aromatic ketones (**2b–d**) and esters (**2e,f**) allowed the synthesis of **4ab–af** in 54–88% yield and 99% ee (entries 7–11).

Scope of Hetero-[6+4] Cycloadditions for Imidazoles and Pyrazoles. Gratifyingly, the described hetero-[6+4] cycloaddition strategy could be extended to imidazoles (**1g,h**) and pyrazoles (**1i**), applying only some minor modifications of the reaction conditions. The scope of the cycloadditions of **1g–i** was demonstrated by reaction with four electron-deficient dienes **2** (Scheme 2). Imidazole-2-carbaldehyde **1g**, as well as imidazole-4-carbaldehyde **1h**, required in most of the cases milder reaction conditions (10 mol% catalyst and additive, and higher dilution) due to some instability of the respective products in the reaction mixtures. The hetero-[6+4] cycloadducts **4ga**, **4gd**, and **4ge** were obtained in moderate to good yields (46–69%) and high enantioselectivities (84–95% ee). In comparison, similar high enantiomeric excesses, but lower yields were obtained for **4ha**, **4hb**, and **4he**, probably due to enhanced instability of these products. Finally, pyrazole-5-carbaldehyde **1i** turned out to be the least reactive heterocycle investigated; however, we were pleased to obtain **4ia** and **4ib** in 31% and 38% yield, and 87% and 90% ee, respectively. For the optimization of the reaction conditions for aldehydes **1g–i** see Supporting Information.

Scope of Hetero-[6+4] Cycloadditions for Dienes 5. In addition, a different class of electron-deficient dienes **5**, based on an acyclic and less conformationally restricted scaffold, was reacted with pyrrole **1a** and imidazole **1g**. These examples required an increased catalyst and additive loading (40 mol%), and a longer reaction time (4 days; for additional optimization, see Supporting Information). Both an electron-neutral aryl substituent (**5a**) and an electron-poor one (**5b**) were tolerated (Scheme 3). Products **6aa** and **6ab**, displaying a different decoration of the seven-membered ring with respect to cycloadducts **4**, were obtained in good yields and excellent enantioselectivities. Furthermore, imidazole **1g** reacted with **5a**, affording **6ga** in moderate yield and slightly diminished

Scheme 2. Scope of the Hetero-[6+4] Cycloadditions of Imidazoles and Pyrazoles 1g–i with Electron-Deficient Dienes 2[a]

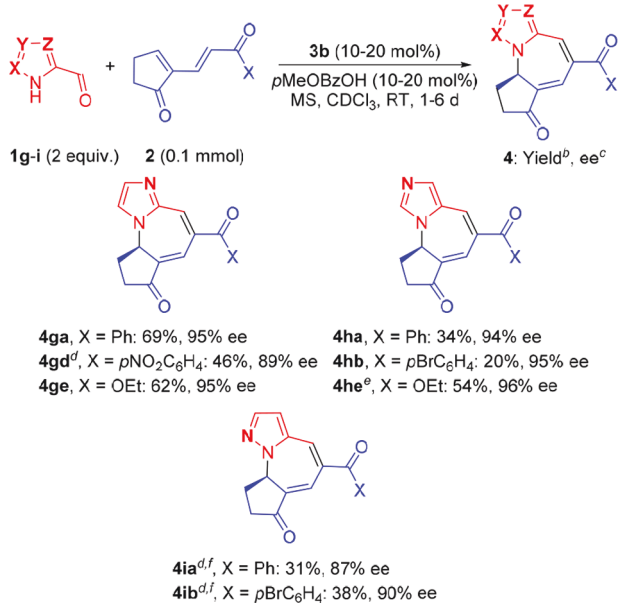

[a]Reaction conditions: Supporting Information. Unless otherwise stated, 10 mol% **3b** and 10 mol% *p*MeOBzOH were employed; reaction time: 1 d. [b]Isolated yield. [c]Determined by chiral stationary phase UPCC. [d]**3b** (20 mol%), *p*MeOBzOH (20 mol%). [e]Reaction time: 2 d. [f]Reaction time: 6 d.

DOI: 10.1021/jacs.8b13659
J. Am. Chem. Soc. 2019, 141, 3288–3297

Scheme 3. Scope of the Hetero-[6+4] Cycloadditions of Pyrrole 1a and Imidazole 1g with Electron-Deficient Dienes 5[a]

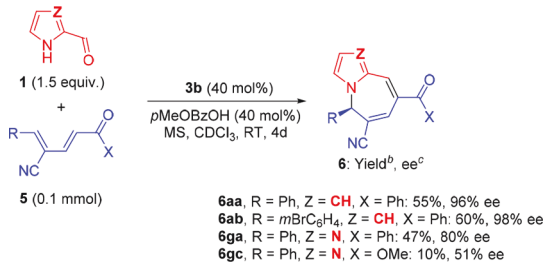

[a]Reaction conditions: Supporting Information. [b]Isolated yield. [c]Determined by chiral stationary phase UPCC.

enantioselectivity. However, the reaction with ester **5c** gave **6gc** in only 10% yield and 51% ee. These examples demonstrate the broad applicability of the methodology for the construction of structurally diverse hetero-[6+4] cycloadducts.

Transformation of Hetero-[6+4] Cycloadduct 4aa. Having explored the reactivity of various substrates toward the hetero-[6+4] cycloaddition reaction, we decided to illustrate the bicyclic system as a useful intermediate in the synthesis of more densely functionalized compounds. The reaction of **4aa** with BnSH in the presence of a catalytic amount of Et_3N afforded compound **4′aa**, bearing three consecutive stereocenters, as a single diastereomer in 57% yield and 99% ee (Scheme 4).

Scheme 4. Transformation of [6+4] Cycloadduct 4aa[a]

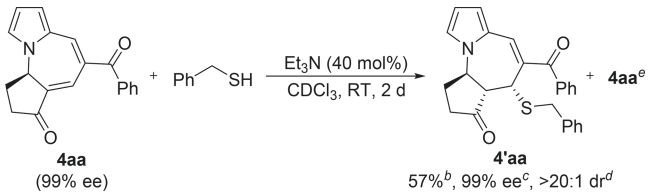

[a]Reaction conditions: Supporting Information. [b]Isolated yield. [c]Determined by chiral stationary phase UPCC. [d]Measured by NMR on the crude reaction mixture. [e]38% recovered starting material (**4aa**).

Screening of Reaction Conditions for Hetero-[6+2] Cycloadditions. We then envisioned to extend this strategy to enantioselective hetero-[6+2] cycloadditions.[44,45] We initially found that pyrrole-2-carbaldehyde **1a** reacted with 1.5 equiv of *trans*-*β*-nitrostyrene **7a** in the presence of catalyst ***ent*-3a** (20 mol%) in $CDCl_3$ at room temperature to produce cycloadduct **8aa** in 40% yield and 66% ee after 48 h (Table 3, entry 1). The addition of BzOH (20 mol%) increased the enantioselectivity (entry 2), and performing the reaction in the presence of MS allowed to reach the same yield in 24 h (entry 3). Employing catalyst **3b**, which was a highly stereoselective catalyst in the hetero-[6+4] cycloaddition, resulted in only a slightly improved yield and similar enantioselectivity (entry 4). Bulkier catalyst **3d** improved the enantioselectivity to 82% ee, without significantly lowering the conversion (entries 5 and 6). See Supporting Information for further screening results. To ease the purification, we inverted the **1a**/**7a** ratio, affording full consumption of **7a**. During this experiment we noticed that compound **8aa** was prone to double bond shift in the reaction

Table 3. Optimization of the Hetero-[6+2] Cycloaddition[a]

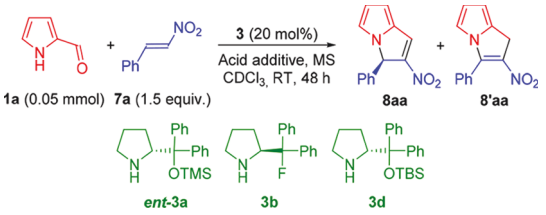

entry	3	additive	yield (conv of 7a, %)[b,c]	ratio 8aa/8′aa[b]	ee (%)[d]
1	*ent*-3a	–[e]	40 (50)	>20:1	66
2	*ent*-3a	BzOH[e,f]	40 (48)	>20:1	76
3[g]	*ent*-3a	BzOH[f]	41 (52)	>20:1	76
4	3b	BzOH[f]	49 (59)	>20:1	−77
5[g]	3d	BzOH[f]	35 (30)	>20:1	82
6	3d	BzOH[f]	50 (65)	18:1	82
7[g,h]	3d	BzOH[i]	40 (80)	13:1	81
8[h]	3d	BzOH[i]	41 (>99)	2.5:1	76
9	3d	BzOH[i]	62 (65)	>20:1	82

[a]Reaction conditions: Supporting Information. [b]Measured by NMR on the crude reaction mixture with Et_4Si as internal standard. [c]Amount of **7a** present in the reaction mixture divided by initial amount. [d]Determined by chiral stationary phase UPCC. [e]No MS added. [f]20 mol% used. [g]Reaction time: 24 h. [h]In this case, the reaction was carried out with an inverted stoichiometric ratio: 1.5 equiv. **1a** employed. [i]10 mol% used.

mixture, leading to isomer **8′aa**. We hypothesized that this shift was acid promoted, leading us to lower its amount to 10 mol%. Even so, we found that this side reaction still occurred, but only when the nitroolefin was consumed (entries 7 and 8). Therefore, an excess of nitroolefin was employed to disfavor the isomerization, thus delivering the optimal conditions (entry 9). Unfortunately, we observed both isomerization and decomposition of **8aa** as isolated compound. At present time, we have not elucidated the pathway of this double bond shift. However, we exclude an equilibration between the two isomers, since recovered **8aa** showed only slightly diminished enantiomeric excess instead of displaying complete racemization. Nonetheless, we surmised that exploiting the reactivity of the electrophilic double bond might circumvent this issue and at the same time bring diversity to the methodology. We therefore conceived a two-step one-pot strategy, consisting in the addition of a nucleophile to the reaction mixture at the end of the hetero-[6+2] cycloaddition step.

Scope and Transformations of Hetero-[6+2] Cycloadducts of Pyrroles. It was found that aryl groups on the pyrrole ring lead to stable hetero-[6+2] cycloadducts. Thus, **8ea** and **8fa**, which were derived from the respective pyrrole-2-carbaldehydes **1e** and **1f** reacting with *trans*-*β*-nitrostyrene **7a**, were isolated in good yields and enantioselectivities (Scheme 5).

In Scheme 5, we demonstrate the hetero-[6+2] cycloaddition of two different pyrrole-2-carbaldehydes with various nitroolefins coupled with a selective reduction with $NaBH_4$ for the preparation of dihydropyrrolizines **9**. This reaction afforded **9aa**, derived from pyrrole-2-carbaldehyde **1a** and *trans*-*β*-nitrostyrene **7a** in 45% overall yield and 82% ee. This protocol was also successfully applied to the hetero-[6+2] cycloaddition of **1a** with 4-bromo- and 4-fluoro-substituted nitroolefins **7b** and **7c** affording **9ab** and **9ac** with similar results. The 4-bromo-substituted pyrrole-2-carbaldehyde **1b**

DOI: 10.1021/jacs.8b13659
J. Am. Chem. Soc. 2019, 141, 3288−3297

Scheme 5. Scope of the Hetero-[6+2] Cycloaddition of Pyrrole-2-carbaldehydes 1 with Nitroolefins 7[a]

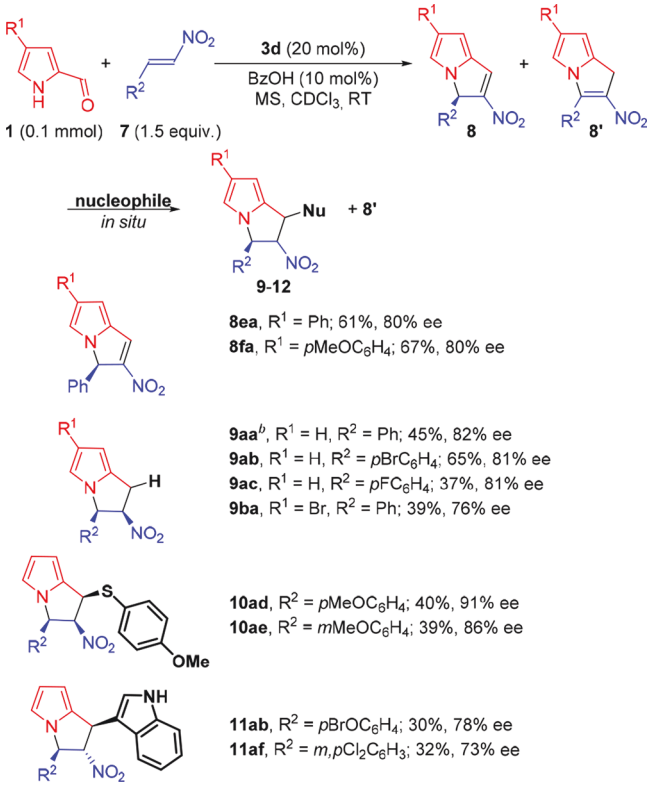

[a]Reaction conditions: Supporting Information. Isolated yield. Enantiomeric excess determined by chiral stationary phase UPCC. [b]Reaction performed on 1 mmol scale.

underwent the same reaction sequence, displaying slightly diminished efficiency. 4-Methoxy- and 3-methoxy-substituted nitroolefins **7d** and **7e** also participated successfully in the hetero-[6+2] cycloaddition with **1a**. Further diversity was demonstrated by addition of 4-methoxythiophenol giving **10ad** and **10ae**, displaying three contiguous stereocenters, as single diastereoisomers, with moderate yields and good enantioselectivities. A neutral nucleophile such as indole was also found to be a competent reaction partner. This protocol was employed to prepare **11ab** and **11af**, obtained as single diastereoisomers. The absolute stereochemistry of compound **8ea** was determined by ECD analysis[46] (see Supporting Information) and extended for analogy to **8**, **9**, **10**, and **11**. For compounds **9**, **10**, and **11**, the stereochemistry of the stereocenters created during the transformations, relative to that of the original stereocenter, was assigned by NMR spectroscopy. The disclosed one-pot hetero-[6+2] cycloaddition–nucleophilic addition sequence—was thus demonstrated to display wide applicability and synthetic utility in the rapid preparation of complex and biologically relevant structures from simple and commercially available starting materials.

MECHANISTIC INVESTIGATIONS

Experimental Investigations. A series of experimental investigations was initiated to gain insight into possible intermediates and reaction pathway(s) involved in the mechanism of the hetero-[6+4] and -[6+2] cycloadditions. A proposed mechanism for the hetero-[6+4] cycloaddition is outlined in Scheme 6.

Scheme 6. Proposed Mechanism for the Formation of Hetero-[6+4] Cycloadducts 4 via Iminium Ion I and Hetero-6π Component II[a]

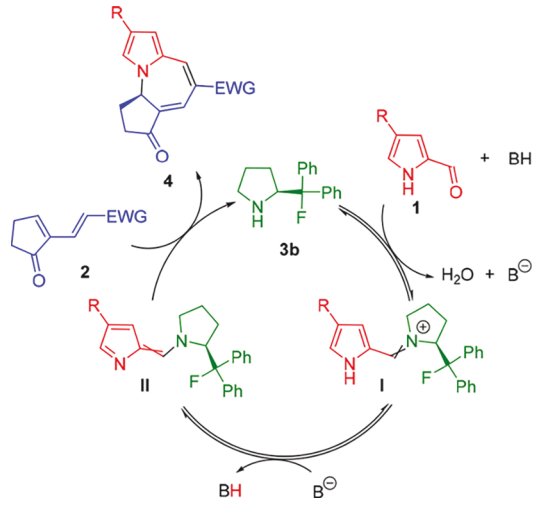

[a]The crossed double bonds refer to a mixture of *cis*- and *trans*-stereoisomers.

The first step of the mechanistic investigations was to identify the proposed intermediates **I** and **II** shown in Scheme 6. We started by attempting to detect the reactive intermediate(s) by means of NMR spectroscopy.[47−49] We treated pyrrole-2-carbaldehyde **1b** with a stoichiometric amount of catalyst **3b** and BzOH in $CDCl_3$ at room temperature over MS for 18 h (Scheme 7, Experiment 1). A new

Scheme 7. Experiments for the Observation of Intermediates I and II and Their Reaction with Diene 2e

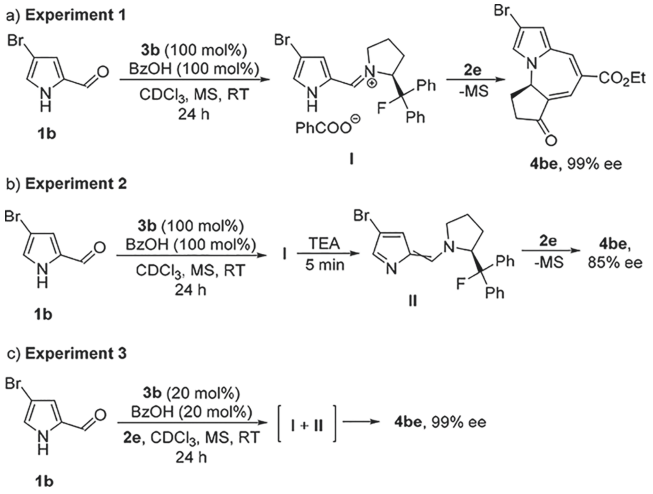

species was observed by ^{1}H NMR, assigned to be iminium ion **I** (see Supporting Information for detailed NMR spectra). Isolation of **I** was impaired by its tendency to rapidly hydrolyze in air.[50] When the electron-deficient diene **2e** was added to the NMR tube, product **4be** (EWG = CO_2Et, 99% ee) was formed, and in parallel, iminium ion **I** disappeared. The absence of MS in the NMR tube considerably slowed down the regeneration of intermediate **I** via condensation of **3b** with **1b**, resulting in increasing catalyst **3b** concentration over time. We thus proved the role of **I** as a productive intermediate for the reaction. By treatment of intermediate **I** with a base, such as triethylamine, another species appeared, showing broad signals in ^{1}H NMR and two distinctive different signals in ^{19}F NMR, suggesting the presence of two isomers (see Supporting Information and computational section). These NMR signals were assigned to intermediate **II**,

DOI: 10.1021/jacs.8b13659
J. Am. Chem. Soc. 2019, 141, 3288−3297

which was also unstable and prone to hydrolysis. Further characterization of intermediate **II** was not possible (Scheme 7, Experiment 2). Then, electron-poor 4π-component **2e** was treated with preformed intermediate **II**, in the absence of MS, and formation of product **4be** was observed (^{1}H NMR), along with consumption of **II** and concomitant catalyst **3b** release (monitored by ^{19}F NMR), suggesting **II** as a second reactive intermediate in the hetero-[6+4] cycloaddition. It should be noted that under these latter stoichiometric reaction conditions and in the presence of triethylamine, performed for the mechanistic investigations, product **4be** was formed in 85% ee, which is lower than the excellent enantioselectivities obtained in the hetero-[6+4] cycloaddition under catalytic conditions.

To better mimic the optimized reaction conditions, we moved to monitor the actual catalytic reaction proceedings by mean of NMR spectroscopy (Scheme 7, Experiment 3, and Figure 2). Pyrrole-2-carbaldehyde **1b** was continuously consumed during the reaction (Figure 2, graph A). The concentration of the catalyst quickly decreased at the beginning of the reaction course, and, since it was regenerated by product formation, its amount reached a steady state (graph B). Interestingly, the rapid formation of iminium ion **I** was observed at first, and ^{19}F NMR revealed the presence of intermediate **II** as well, in about 3:1 ratio in favor of **I**. Intermediate **I** reached a steady state after a rapid build-up (graph C) and remained constant for several hours, while product **4be** was slowly forming (graph D). During these investigations, intermediate **II** appeared as two distinct signals, confirming the presence of two isomers. The importance of MS was also underlined by this experiment, as they allowed constant replacement of the reacted intermediates by facilitating the condensation of catalyst **3b** and **1b**. Observability of intermediates **I** and **II** in an experiment performed under the real optimized reaction conditions (i.e., their formation was not forced), indicates compelling evidence of these species being reactive intermediates in the hetero-[6+4] cycloaddition.

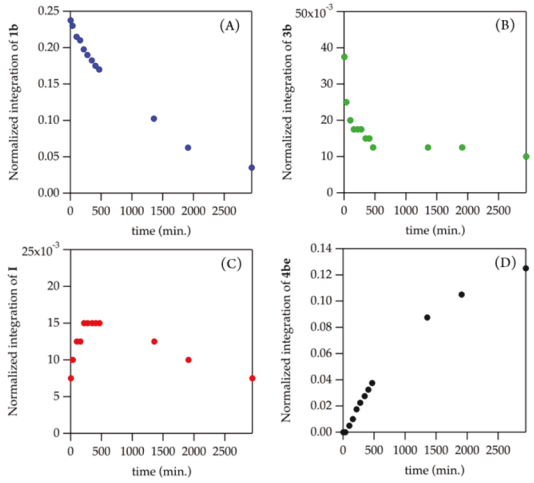

Figure 2. (A) Consumption of pyrrole-2-carbaldehyde **1b** as a function of time. (B) Amount of catalyst **3b** over time. (C) Development of iminium ion **I** over time. (D) Cycloadduct **4be** formation as a function of time. Reaction conditions: pyrrole-2-carbaldehyde **1b** (1 equiv), diene **2e** (1 equiv), catalyst **3b** (20 mol%), and BzOH (20 mol%) in $CDCl_3$ (0.17 M), in the presence of MS. Integrations have been normalized toward Et_4Si as internal standard.

Computational Investigations. The energies of iminium ion **I** and intermediate **II**, and the details of mechanisms, were investigated with density functional theory. Computations were performed with M06-2X[51]/def2-TZVPP[52] corrected energies with the SMD[53] ($CHCl_3$) solvation model on B3LYP[54−57]/6-31G(d) calculated geometries (see the Supporting Information for details on computational methods).

Intermediate Structures. The lowest-energy conformations for the *trans*- and *cis*-iminium ion are shown in Figure 3. The difference in free energy is 3.2 kcal/mol, in favor of the *trans*-iminium ion. The *cis*-iminium ion acquires a disfavored conformation of the catalyst to accommodate the pyrrole substituent (the high-energy catalyst is shown in Figure 3). This corroborates the NMR observation of one signal for iminium ion **I**. The *cis*- and *trans*-6π-components were also calculated. We found that their difference in free energy was 1.1 kcal/mol in favor of the *cis*-6π-component. This also agrees with the observation of two signals for intermediate **II**, where both *cis*- and *trans*-6π-components are observable by NMR spectroscopy.

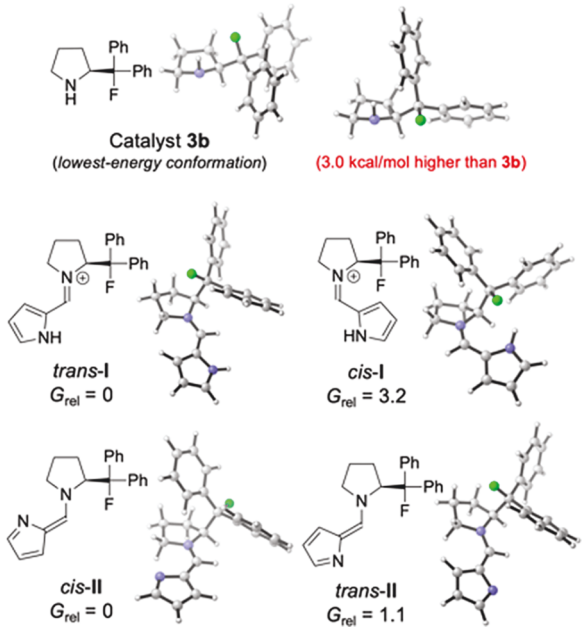

Figure 3. Optimized ground-state structures for two conformations of catalyst **3b** and lowest-energy conformations for the *cis*- and *trans*-arrangements of intermediates **I** and **II**(M06-2X/def2-TZVPP-SMD//B3LYP/6-31G(d)-SMD, $CHCl_3$).

Calculation of the Enantioselective Hetero-[6+4] Cycloaddition Pathway. To probe the mechanism of the hetero-[6+4] cycloadditions, DFT calculations were performed to locate the transition states of the reaction of the 6π-components **II** and a slightly truncated model of substrate **2**. This truncation modified the aryl or ester group on the terminal carbonyl to a methyl to avoid conformational flexibility. The concerted cycloaddition transition structures were exhaustively searched (see Figure S9), but only revealed stepwise pathways.

We computed the free energy profile for the reaction mechanism after the hetero-6π-components **II** are formed (Figure 4). The zero-energy refers to the separated hetero-6π-components **II** and substrate **2**. The first step involves nucleophilic addition of the pyrrole nitrogen to the electrophilic β-position of the cyclic enone. The two lowest-energy transition structures leading to the two stereoisomers are **TS-Ia** and **TS-Ib** (see Figure S10 for the set of the various transition structure conformations). Transition structure **TS-Ia** provides the (*R*)-zwitterionic intermediate (*R*)-**int-Ia** which leads to the observed stereoisomer with a free energy of activation barrier of 23.4 kcal/mol. Transition structure **TS-Ib** yields the corresponding (*S*)-intermediate and minor stereoisomer with a free energy of activation barrier of 22.8 kcal/mol. Interestingly, both low-energy TSs are nucleophilic additions via the pyrrole nitrogen lone pair instead of the π-system. Both transition structures arise from the *trans*-**II** hetero-6π-component. All transition structures from *cis*-**II** were at least 3.0 kcal/mol higher in energy (see Figure S10). We found the difference in energy between **TS-Ia** and **TS-Ib** to be 0.6 kcal/mol, in favor of **TS-Ib**. We predict the two zwitterions, (*R*)-**int-Ia** and (*S*)-**int-Ib**, to

DOI: 10.1021/jacs.8b13659
J. Am. Chem. Soc. 2019, 141, 3288−3297

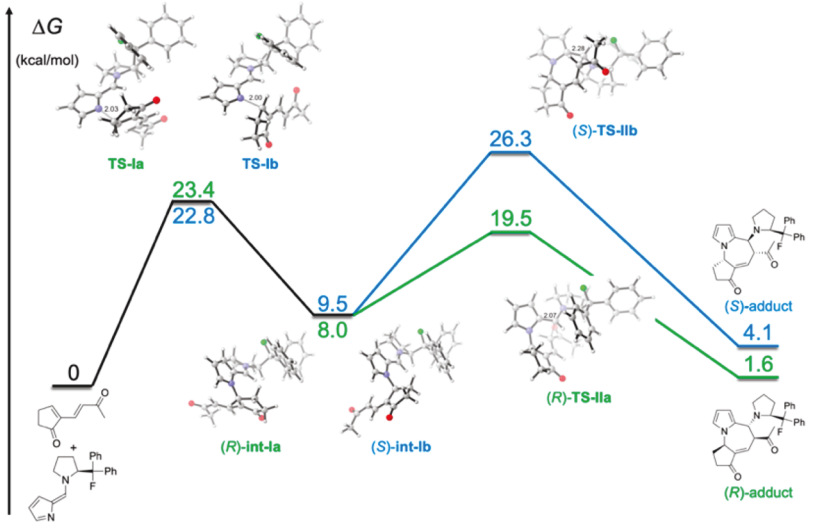

Figure 4. Computed free energy reaction pathway profile for the hetero-[6+4] cycloaddition involving hetero-6-π-intermediate *trans*-**II** derived from catalyst **3b** and model of substrate **2** (M06-2X/def2-TZVPP-SMD//B3LYP/6-31G(d)-SMD, $CHCl_3$). The starting point is the computed free energy of the separated *trans*-**II** and substrate, and all following energies are compared to them. All structures are lowest-energy conformations of transition states or ground states.

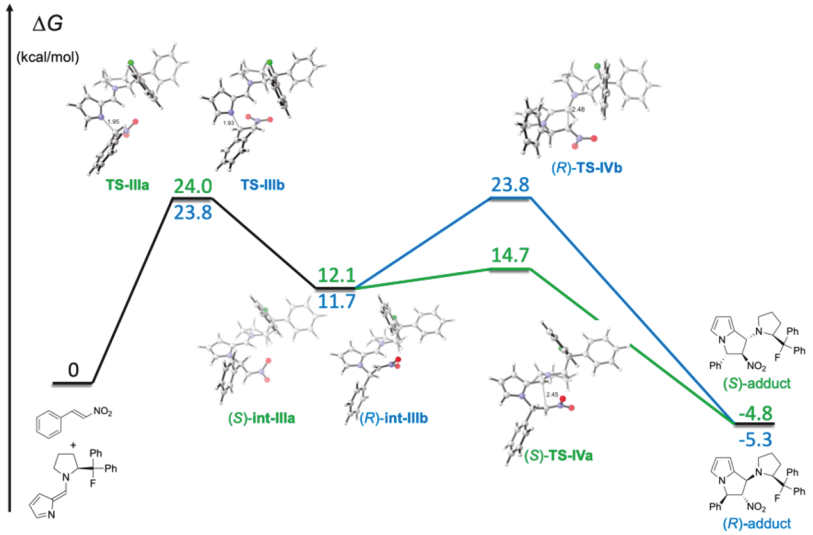

Figure 5. Computed free energy reaction pathway profile for the hetero-[6+2] cycloaddition involving hetero-6-π-intermediate *trans*-**II** derived from catalyst **3b** and substrate **7a** (M06-2X/def2-TZVPP-SMD//B3LYP/6-31G(d)-SMD, $CHCl_3$). The starting point is the computed free energy of the separated *trans*-**II** and substrate, and all following energies are compared to them. All structures are lowest-energy conformations of transition states or ground states.

form in approximately a 74:26 ratio. The zwitterions are 8.0 and 9.5 kcal/mol higher in energy than the separated (*R*)- and (*S*)-intermediates, respectively.

From the zwitterionic intermediate, the cyclization via C−C bond formation occurs by addition of the conjugated enolate to the carbon of the iminium ion. The lowest-energy transition structures for the cyclization of the major and minor stereoisomers are shown in Figure 4 (see Figure S11 for full set of transition structures). The lowest-energy TS, (*R*)-**TS-IIa** leads to the observed adduct with a free energy of activation barrier of 19.5 kcal/mol, which eliminates to the product (not computed). The lowest-energy TS leading to the minor stereoisomer, (*S*)-**TS-IIb**, has a free energy of activation barrier of 26.3 kcal/mol. Transition structure (*S*)-**TS-IIb** is disfavored due to the *s-cis* arrangement of the iminium ion and high-energy conformation of the pyrrolidine catalyst (see high-energy catalyst conformation in Figure 3). The source of these unstable interactions arises from the ketone position in the C−C bond TS. In (*R*)-**TS-IIa**, the ketone is on the opposite side of the bulky pyrrolidine substituent, whereas in (*S*)-**TS-IIb** the ketone points directly at the diphenyl fluoro group, forcing the conformational changes. In summary, the stereoselectivity is controlled by the C−C bond-forming step - the second reactive event in the stepwise mechanism. The N−C bond-forming step yields both (*R*)- and (*S*)-intermediates; however, only (*R*)-**int-Ia** cyclizes readily to the adduct. The barrier for cyclization for (*S*)-**TS-IIb** is significantly higher than the reverse reaction back to the reactants ($\Delta\Delta G^{\ddagger}$ = 3.5 kcal/mol), which causes (*S*)-**int-Ib** to reverse until it is completely consumed and converted to the (*R*)-adduct. This reaction barrier corresponds with the experimental results, where only the (*R*)-product is observed. Calculations using catalyst **3c** reveal a decreased difference in the free energy barriers between forward cyclization and reverse, for the zwitterionic intermediate leading to the minor enantiomer ($\Delta\Delta G^{\ddagger}$ = 2.8 kcal/mol) in agreement with the 95% ee (Table 1, entry 3). This is due to removing the disfavored F···O interaction found in (*S*)-**TS-IIb** (see Figure S12 for the transition structure).

DOI: 10.1021/jacs.8b13659
J. Am. Chem. Soc. 2019, 141, 3288−3297

Calculation of the Enantioselective Hetero-[6+2] Cycloaddition Pathway. While the hetero-[6+4] cycloadditions are practically stereospecific for the reactions with the electron-deficient dienes **2**, the hetero-[6+2] cycloaddition variant is modest in enantioselectivity. We examined the example in Table 3, entry 4, due to its close similarity with the hetero-[6+4] cycloaddition system (same catalyst used (**3b**)) to determine the drop in enantioselectivity to 77% ee. We performed exhaustive computational modeling of the mechanism (see Figures S13 for full sets of TSs), and the free energy profile for lowest-energy TSs and intermediates is shown in Figure 5. The two lowest-energy transition structures for the first N−C bond-forming step, **TS-IIIa** and **TS-IIIb**, are within 0.2 kcal/mol, similar to the hetero-[6+4] cycloaddition. They have a free energy of activation barriers of 23.8 and 24.0 kcal/mol for the (*R*)- and (*S*)-pathways, respectively. The two stereoisomeric intermediates, (*S*)-**int-IIIa** and (*R*)-**int-IIIb**, are formed. In this case, (*S*)-**int-IIIa** cyclizes readily with a free energy of activation barrier of 14.7 kcal/mol compared to the separated reactants (2.6 kcal/mol from the intermediate) to form the (*S*)-adduct. In contrast, the barrier for cyclization to form the (*R*)-adduct is 23.8 kcal/mol via (*R*)-**TS-IVb**, equivalent to the N−C bond-forming barrier for the (*R*)-pathway. This TS is unfavorable due to the steric interaction between the nitro group and the phenyl of the pyrrolidine.

Unlike the [6+4] cycloaddition, the nitro group is small enough not to force a conformational change in the catalyst in the [6+2] cycloaddition, and the destabilization of (*R*)-**TS-IVb** is not as pronounced as for (*S*)-**TS-IIb**. The free energy barrier for (*R*)-**TS-IVb** is equal to the N−C bond-forming step for the (*R*)-pathway. To summarize, the N−C bond formation occurs without stereoselectivity and yields both zwitterionic intermediates. The (*S*)-adduct forms rapidly, whereas the (*R*)-intermediate (*R*)-**int-IIIb** has equal barriers to form the adduct or reverse to the reactants, leading to a 2:1 ratio of (*R*)- to (*S*)-stereoisomers. In comparison to the hetero-[6+4] cycloaddition with diene **2**, which is stereospecific, the hetero-[6+2] cycloaddition achieves modest enantioselectivity due to the smaller size of the nitroolefin **7** in the C−C transition state.

Based on these computational results, we anticipated that destabilizing the minor pathway transition structure for the C−C bond (*R*)-**TS-IVb** would improve the enantioselectivity. We predicted that substitution at the 3,5-positions of the pyrrolidine phenyl groups could provide an unfavorable steric environment around the nitro group in (*R*)-**TS-IVb**. This substitution would not interfere with the other stereoisomeric C−C bond-forming TS (*S*)-**TS-IVa**, as well as both the N−C bond-forming TSs. A 3,5-$Me_2C_6H_3$-substituted pyrrolidine catalyst **3e** was synthesized to test the prediction (Scheme 8). The reaction of **1a** and *trans*-*β*-nitrostyrene **7a** with catalyst **3e** afforded the corresponding cycloadduct ***ent*-8aa** with improved enantioselectivity of 85% ee (Scheme 8), supporting the computational prediction. The transition structure for the disfavored C−C bond-forming transition structure **TS-3e-a** is also shown in Scheme 8 with a free energy barrier of 25.0 kcal/mol, showing the increased steric repulsion between the nitro group the methyl substituents introduced in catalyst **3e**.

Scheme 8. Experiments for the Predicted Catalyst 3e and Calculated Transition Structure

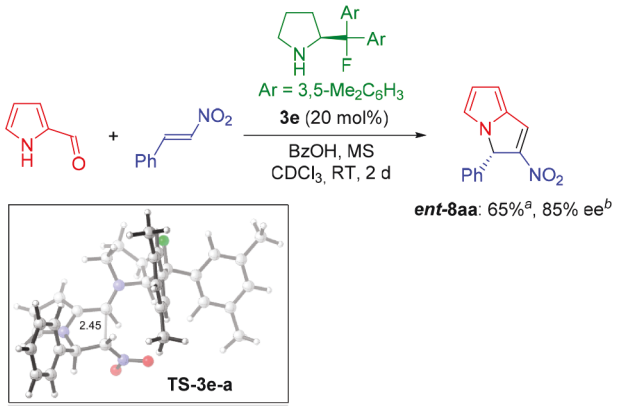

[a]Isolated yield. [b]Enantiomeric excess determined by chiral stationary phase UPCC.

CONCLUSION

We have developed a novel catalytic enantioselective activation of heteroaromatic compounds, such as pyrroles, imidazoles, and pyrazoles, by organocatalysis. This builds upon the generation of electron-rich hetero-6*π* intermediates acting as nucleophiles. These intermediates react in a highly chemo-, regio-, and stereoselective manner with various types of electron-deficient dienes and olefins, in hetero-[6+4] and -[6+2] cycloaddition reactions, respectively. The reaction of pyrroles provides bio-attractive pyrrolo-azepine scaffolds by a [6+4] cycloaddition with dienes, in high yields and excellent enantioselectivities (99% ee). Imidazolo- and pyrazolo-azepines are formed in a similar hetero-[6+4] cycloaddition by reaction of imidazoles and pyrazoles with dienes. The activation concept for pyrroles has been extended to enantioselective hetero-[6+2] cycloaddition reactions with nitroolefins, affording pyrrolizidine alkaloid scaffolds that are demonstrated to undergo further reactions. By NMR investigations, we have been able to identify two different types of intermediates in the catalytic cycle. First, an iminium ion intermediate is formed; then deprotonation of the heteroaromatic N−H leads to the reactive electron-rich hetero-6*π* intermediate formed in two isomeric forms, of which only one reacts with the diene or the olefin in the hetero-[6+4] and -[6+2] cycloadditions, respectively. Mechanistic and computational studies have shown that the hetero-[6+4] and -[6+2] cycloadditions occur via stepwise mechanisms. The stereocontrol occurs at the second C−C bond-forming step, rather than the first N−C bond-forming transition state. The source of stereoselectivity is the difference in free energy of activation barriers between the C−C and N−C TSs for the minor stereoisomer, rather than the traditional comparison between two stereoisomeric transition structures, because of reversibility of the first step. In the case of the hetero-[6+4] cycloaddition, high stereoselectivity is achieved due to the bulky 4*π*-substrate which interacts strongly with the substituent of the pyrrolidine catalyst. For the hetero-[6+2] cycloaddition system, the smaller nitrovinyl substrate does not cause large steric effects at the pyrrolidine catalyst, which lowers the C−C bond-forming TS and achieves lower enantioselectivity compared to the hetero-[6+4] cycloaddition. Computational investigations predicted a catalyst modification that could improve the enantioselectivity for the [6+2] cycloadditions, and experiments showed an increase in the enantioselectivity from 77% to 85% ee.

ASSOCIATED CONTENT

Supporting Information

The Supporting Information is available free of charge on the ACS Publications website at DOI: 10.1021/jacs.8b13659.

Crystallographic data for **4da** (CIF)

Experimental procedures, coordinates of all calculated structures, and product characterization data (PDF)

DOI: 10.1021/jacs.8b13659
J. Am. Chem. Soc. 2019, 141, 3288−3297

AUTHOR INFORMATION

Corresponding Authors

*houk@chem.ucla.edu
*kaj@chem.au.dk

ORCID

Adam Simon: 0000-0001-6334-3359
K. N. Houk: 0000-0002-8387-5261

Notes

The authors declare no competing financial interest.

ACKNOWLEDGMENTS

This work was made possible by generous support from Carlsberg Foundation "Semper Ardens", FNU, Aarhus University and DNRS. K.N.H. and A.S. thank the National Science Foundation (CHE-1764328) for financial support. The authors would like to thank Jeremy D. Erickson for X-ray analysis as well as Teresa A. Palazzo and Danny K. B. Jørgensen for ECD analysis. A.S. thanks the NIH Chemistry-Biology Interface Research Training Grant (T32GM008496) and the UCLA Dissertation Year Fellowship for funding. This work used computational and storage resources associated with the Hoffman2 Shared Cluster provided by the UCLA Institute of Digital Research and Education (IDRE). This work also used the Extreme Science and Engineering Discovery Environment (XSEDE).

REFERENCES

(1) Bhardwaj, V.; Gumber, D.; Abbot, V.; Dhiman, S.; Sharma, P. Pyrrole: A Resourceful Small Molecule in Key Medicinal Heteroaromatics. *RSC Adv.* **2015**, *5*, 15233−15266.

(2) Baltazzi, E.; Krimen, L. I. Recent Advances in the Chemistry of Pyrrole. *Chem. Rev.* **1963**, *63*, 511−556.

(3) Estévez, V.; Villacampa, M.; Menéndez, J. C. Recent Advances in the Synthesis of Pyrroles by Multicomponent Reactions. *Chem. Soc. Rev.* **2014**, *43*, 4633−4657.

(4) Walsh, C. T.; Garneau-Tsodikova, S.; Howard-Jones, A. R. Biological Formation of Pyrroles: Nature's Logic and Enzymatic Machinery. *Nat. Prod. Rep.* **2006**, *23*, 517−531.

(5) Mal, D.; Shome, B.; Dinda, B. K. Pyrrole and its Derivatives. In *Heterocycles in Natural Product Synthesis*; Majumdar, K. C., Chattopadhyay, S. K., Eds.; Wiley-VCH: New York, 2011; pp 313−544.

(6) McNeill, R.; Siudak, R.; Wardlaw, J. H.; Weiss, D. E. Electronic Conduction in Polymers. I. The Chemical Structure of Polypyrrole. *Aust. J. Chem.* **1963**, *16*, 1056−1075.

(7) MacDiarmid, A. G. Synthetic Metals": A Novel Role for Organic Polymers (Nobel Lecture). *Angew. Chem., Int. Ed.* **2001**, *40*, 2581−2590.

(8) Janata, J.; Josowicz, M. Conducting Polymers in Electronic Chemical Sensors. *Nat. Mater.* **2003**, *2*, 19−24.

(9) Liang, X.; Li, Y.; Li, X.; Jing, L.; Deng, Z.; Yue, X.; Li, C.; Dai, Z. PEGylated Polypyrrole Nanoparticles Conjugating Gadolinium Chelates for Dual-Modal MRI/Photoacoustic Imaging Guided Photothermal Therapy of Cancer. *Adv. Funct. Mater.* **2015**, *25*, 1451−1462.

(10) Katritzky, A. R.; Ramsden, C. A.; Joule, J. A.; Zhdankin, V. V., Reactivity of Five-Membered Rings with One Heteroatom. *Handbook of Heterocyclic Chemistry*; Elsevier, 2010; pp 383−472.

(11) Paras, N. A.; MacMillan, D. W. C. New Strategies in Organic Catalysis: The First Enantioselective Organocatalytic Friedel−Crafts Alkylation. *J. Am. Chem. Soc.* **2001**, *123*, 4370−4371.

(12) Trost, B. M.; Müller, C. Asymmetric Friedel−Crafts Alkylation of Pyrroles with Nitroalkenes Using a Dinuclear Zinc Catalyst. *J. Am. Chem. Soc.* **2008**, *130*, 2438−2439.

(13) Zhang, D.; Qiu, H.; Jiang, L.; Lv, F.; Ma, C.; Hu, W. Enantioselective Palladium(II) Phosphate Catalyzed Three Component Reactions of Pyrrole, Diazoesters, and Imines. *Angew. Chem., Int. Ed.* **2013**, *52*, 13356−13360.

(14) Beeson, T. D.; Mastracchio, A.; Hong, J.-B.; Ashton, K.; MacMillan, D. W. C. Enantioselective Organocatalysis Using SOMO Activation. *Science* **2007**, *316*, 582−585.

(15) Lee, H.-J.; Cho, C.-W. Cinchona-Based Primary Amine-Catalyzed Asymmetric Cascade Aza-Michael−Aldol Reactions of Enones with 2-(1*H*-Pyrrol-2-yl)-2-oxoacetates: Synthesis of Chiral Pyrrolizines with Multistereocenters. *J. Org. Chem.* **2013**, *78*, 3306−3312.

(16) Bae, J.-Y.; Lee, H.-J.; Youn, S.-H.; Kwon, S.-H.; Cho, C.-W. Organocatalytic Asymmetric Synthesis of Chiral Pyrrolizines by Cascade Conjugate Addition−Aldol Reactions. *Org. Lett.* **2010**, *12*, 4352−4355.

(17) Lee, H.-J.; Cho, C.-W. Asymmetric Synthesis of Chiral Pyrrolizine-Based Triheterocycles by Organocatalytic Cascade Aza-Michael−Aldol Reactions. *Eur. J. Org. Chem.* **2014**, *2014*, 387−394.

(18) Li, P.; Fang, F.; Chen, J.; Wang, J. Organocatalytic Asymmetric Aza-Michael Addition of Pyrazole to Chalcone. *Tetrahedron: Asymmetry* **2014**, *25*, 98−101.

(19) Fu, N.; Zhang, L.; Luo, S.; Cheng, J.-P. Chiral Primary Amine Catalysed Asymmetric Conjugate Addition of Azoles to α-Substituted Vinyl Ketones. *Org. Chem. Front.* **2014**, *1*, 68−72.

(20) Zhang, J.; Zhang, Y.; Liu, X.; Guo, J.; Cao, W.; Lin, L.; Feng, X. Enantioselective Protonation by Aza-Michael Reaction between Pyrazoles and α-Substituted Vinyl Ketones. *Adv. Synth. Catal.* **2014**, *356*, 3545−3550.

(21) Mose, R.; Preegel, G.; Larsen, J.; Jakobsen, S.; Iversen, E. H.; Jørgensen, K. A. Organocatalytic Stereoselective [8+2] and [6+4] Cycloadditions. *Nat. Chem.* **2016**, *9*, 487−492.

(22) Donslund, B. S.; Monleón, A.; Palazzo, T. A.; Christensen, M. L.; Dahlgaard, A.; Erickson, J. D.; Jørgensen, K. A. Organocatalytic Enantioselective Higher-Order Cycloadditions of In Situ Generated Amino Isobenzofulvenes. *Angew. Chem., Int. Ed.* **2018**, *57*, 1246−1250.

(23) Wang, S.; Rodríguez-Escrich, C.; Pericàs, M. A. Catalytic Asymmetric [8+2] Annulation Reactions Promoted by a Recyclable Immobilized Isothiourea. *Angew. Chem., Int. Ed.* **2017**, *56*, 15068−15072.

(24) Donslund, B.; Jessen, N. I.; Bertuzzi, G.; Giardinetti, M.; Palazzo, T. A.; Christensen, M. L.; Jørgensen, K. A. Catalytic Enantioselective [10+4] Cycloadditions. *Angew. Chem., Int. Ed.* **2018**, *57*, 13182−13186.

(25) Hayashi, Y.; Gotoh, H.; Honma, M.; Sankar, K.; Kumar, I.; Ishikawa, H.; Konno, K.; Yui, H.; Tsuzuki, S.; Uchimaru, T. Organocatalytic, Enantioselective Intramolecular [6+2] Cycloaddition Reaction for the Formation of Tricyclopentanoids and Insight on Its Mechanism from a Computational Study. *J. Am. Chem. Soc.* **2011**, *133*, 20175−20185.

(26) Hong, B.-C.; Shr, Y.-J.; Wu, J.-L.; Gupta, A. K.; Lin, K.-J. Novel [6+2] Cycloaddition of Fulvenes with Alkenes: A Facile Synthesis of the Anislactone and Hirsutane Framework. *Org. Lett.* **2002**, *4*, 2249−2252.

(27) Hong, B.-C.; Sun, H.-I; Chen, Z.-Y. Unprecedented and Novel Hetero [6+3] Cycloadditions of Fulvene: A Facile Synthesis of the 11-Oxasteroid Framework. *Chem. Commun.* **1999**, 2125−2126.

(28) Hong, B.-C.; Jiang, Y.-F.; Kumar, E. S. Microwave-assisted [6+4]-Cycloaddition of Fulvenes and α-Pyrones to Azulene−indoles: Facile Syntheses of Novel Antineoplastic Agents. *Bioorg. Med. Chem. Lett.* **2001**, *11*, 1981−1984.

(29) Zhou, Z.; Wang, Z.-X.; Zhou, Y.-C.; Xiao, W.; Ouyang, Q.; Du, W.; Chen, Y.-C. Switchable Regioselectivity in Amine-catalysed Asymmetric Cycloadditions. *Nat. Chem.* **2017**, *9*, 590−594.

(30) Przydacz, A.; Skrzyńska, A.; Albrecht, Ł. Breaking Aromaticity with Aminocatalysis: A Convenient Strategy for Asymmetric Synthesis. *Angew. Chem., Int. Ed.* **2019**, *58*, 63.

DOI: 10.1021/jacs.8b13659
J. Am. Chem. Soc. 2019, 141, 3288−3297

(31) Xiao, B.-X.; Gao, X.-Y.; Du, W.; Chen, Y.-C. Asymmetric Reactions Involving Lewis Base Catalyst Tethered Dearomatized Intermediates. *Chem. - Eur. J.* **2019**, *25*, 1607.
(32) Watanabe, M.; Kobayashi, T.; Kajigaeshi, S.; Kanemasa, S. Azafulvenes 1. A Novel Generative Method of 6-Amino-1-Azafulvene and its Cycloaddition Reaction with Isothiocyanate. *Chem. Lett.* **1975**, *4*, 607−610.
(33) Galeazzi, E.; Guzman, A.; Rodriguez, G.; Muchowski, J. M. Generation and Lithiation of the Dimers of 6-(Dimethylamino)-1,4-diazafulvene. A Novel Synthesis of 2-Alkanoylimidazoles. *J. Org. Chem.* **1993**, *58*, 974−976.
(34) Barluenga, J.; García-Rodríguez, J.; Martínez, S.; Suárez-Sobrino, A. L.; Tomás, M. Facile and Versatile Annulation of the Imidazole Ring: Single and Sequential Cyclization Reactions of Fischer Carbene Complexes with 1,4-Diazafulvenes. *Chem. - Eur. J.* **2006**, *12*, 3201−3210.
(35) Huang, S.-Z.; Kong, F.-D.; Ma, Q.-Y.; Guo, Z.-K.; Zhou, L.-M.; Wang, Q.; Dai, H.-F.; Zhao, Y.-X. Nematicidal Stemona Alkaloids from Stemona Parviflora. *J. Nat. Prod.* **2016**, *79*, 2599−2605.
(36) Paudler, W. W.; Kerley, G. I.; McKay, J. The Alkaloids of Cephalotaxus Drupacea and Cephalotaxus Fortunei. *J. Org. Chem.* **1963**, *28*, 2194−2197.
(37) Walser, A.; Fryer, R. I. Imidazodiazepines and Processes Therefor. U.S. Patent US4280957 (A), July 28, 1981.
(38) Rizk, A.-F. *Naturally Occurring Pyrrolizidine Alkaloids*; CRC Press: Boca Raton, FL, 1990.
(39) Harrington, P. J.; Khatri, H. N.; Schloemer, G. C. Preparation of Ketorolac. U.S. Patent US6323344 (B1), November 27, 2001.
(40) Marigo, M.; Wabnitz, T. C.; Fielenbach, D.; Jørgensen, K. A. Enantioselective Organocatalyzed α-Sulfenylation of Aldehydes. *Angew. Chem., Int. Ed.* **2005**, *44*, 794−797.
(41) Hayashi, Y.; Gotoh, H.; Hayashi, T.; Shoji, M. Diphenylprolinol Silyl Ethers as Efficient Organocatalysts for the Asymmetric Michael Reaction of Aldehydes and Nitroalkenes. *Angew. Chem., Int. Ed.* **2005**, *44*, 4212−4215.
(42) Ho, C.-Y.; Chen, Y.-C.; Wong, M.-K.; Yang, D. Fluorinated Chiral Secondary Amines as Catalysts for Epoxidation of Olefins with Oxone. *J. Org. Chem.* **2005**, *70*, 898−906.
(43) Sparr, C.; Schweizer, B.; Senn, H. M.; Gilmour, R. The Fluorine-Iminium Ion *Gauche* Effect: Proof of Principle and Application to Asymmetric Organocatalysis. *Angew. Chem., Int. Ed.* **2009**, *48*, 3065−3068.
(44) Takaoka, K.; Aoyama, T.; Shioiri, T. Cycloaddition Reactions of Trimethylsilylketene with 8-Azaheptafulvenes and 6-Amino-1-azafulvenes. *Heterocycles* **2001**, *54*, 209−215.
(45) For a very low enantioselectivity seminal work, see: Yin, G.; Zhang, R.; Li, L.; Tian, J.; Chen, L. One-Pot Enantioselective Synthesis of 3-Nitro-2*H*-chromenes Catalyzed by a Simple 4-Hydroxyprolinamide with 4-Nitrophenol as Cocatalyst. *Eur. J. Org. Chem.* **2013**, *2013*, 5431−5438.
(46) Stephens, P. J.; Devlin, F. J.; Chabalowski, C. F.; Frisch, M. J. *Ab Initio* Calculation of Vibrational Absorption and Circular Dichroism Spectra Using Density Functional Force Fields. *J. Phys. Chem.* **1994**, *98*, 11623−11627.
(47) Sonnet, P. E. Synthesis of β-Substituted Pyrroles *via* 1-(Pyrrol-2-ylmethylene)pyrrolidinium Salts. *J. Org. Chem.* **1971**, *36*, 1005−1007.
(48) Berthiaume, S. L.; Bray, B. L.; Hess, P.; Liu, Y.; Maddox, M. L.; Muchowski, J. M.; Scheller, M. E. Synthesis of 5-substituted Pyrrole-2-carboxaldehydes. Part I. Generation of Formal 5-Lithiopyrrole-2-carboxaldehyde Equivalents by Bromine-lithium Exchange of 2-Bromo-6-(diisopropylamino)-1-azafulvene Derivatives. *Can. J. Chem.* **1995**, *73*, 675−684.
(49) Sonnet, P. E.; Flippen, J. L.; Gilardi, R. D. Substituted 1-(Pyrrol-2-ylmethylene)pyrrolidinium Salts a Source of Stable 2-Azafulvenamines. *J. Heterocycl. Chem.* **1974**, *11*, 811−812.
(50) Residual traces of water are responsible for partial hydrolysis of the iminium ion, explaining why we could never obtain this intermediate quantitatively.
(51) Zhao, Y.; Truhlar, D. G. The M06 Suite of Density Functionals for Main Group Thermochemistry, Thermochemical Kinetics, Noncovalent Interactions, Excited States, and Transition Elements: Two New Functionals and Systematic Testing of Four M06-class Functionals and 12 other Functionals. *Theor. Chem. Acc.* **2008**, *120*, 215−241.
(52) Weigend, F.; Ahlrichs, R. Balanced Basis Sets of Split Valence, Triple Zeta Valence and Quadruple Zeta Valence Quality for H to Rn: Design and Assessment of Accuracy. *Phys. Chem. Chem. Phys.* **2005**, *7*, 3297−3305.
(53) Marenich, A. V.; Cramer, C. J.; Truhlar, D. G. Universal Solvation Model Based on Solute Electron Density and on a Continuum Model of the Solvent Defined by the Bulk Dielectric Constant and Atomic Surface Tensions. *J. Phys. Chem. B* **2009**, *113*, 6378−6396.
(54) Vosko, S. H.; Wilk, L.; Nusair, M. Accurate Spin-dependent Electron Liquid Correlation Energies for Local Spin Density Calculations: a Critical Analysis. *Can. J. Phys.* **1980**, *58*, 1200−1211.
(55) Lee, C.; Yang, W.; Parr, R. G. Development of the Colle-Salvetti Correlation-Energy Formula into a Functional of the Electron Density. *Phys. Rev. B: Condens. Matter Mater. Phys.* **1988**, *37*, 785−789.
(56) Becke, A. D. Density-functional Thermochemistry. III. The Role of Exact Exchange. *J. Chem. Phys.* **1993**, *98*, 5648−5652.
(57) Stephens, P. J.; Devlin, F. J.; Chabalowski, C. F.; Frisch, M. J. Ab Initio Calculation of Vibrational Absorption and Circular Dichroism Spectra using Density Functional Force Fields. *J. Phys. Chem.* **1994**, *98*, 11623−11627.

DOI: 10.1021/jacs.8b13659
J. Am. Chem. Soc. 2019, 141, 3288−3297